

Formation and Thermally-Induced Disruption of Nanowhiskers in Poly(3-hexylthiophene)/Xylene Gel Studied by Small-Angle X-ray Scattering

Chun-Yu Chen,[†] Shu-Hua Chan,^{†,‡} Jian-Yi Li,[§] Kuan-Han Wu,[§] Hsin-Lung Chen,^{*,†}
Jean-Hong Chen,^{*,§} Wen-Yao Huang,[⊥] and Show-An Chen[†]

[†]Department of Chemical Engineering, National Tsing Hua University, Hsin-Chu 30013, Taiwan,

[‡]Materials and Chemical Laboratories, Industrial Technology Research Institute, Chutung, Hsin-Chu, 310, Taiwan, [§]Department of Polymer Materials, Kun Shan University, Tainan Hsien 71003, Taiwan, and

[⊥]Department of Photonics, National Sun Yat-sen University, Kaohsiung 804, Taiwan

Received April 13, 2010; Revised Manuscript Received July 19, 2010

ABSTRACT: We identified the formation of nanowhiskers of poly(3-hexylthiophene) (P3HT) in the gel with xylene *in situ* by means of small-angle X-ray scattering (SAXS). In the freshly prepared solution, the rodlike segments of P3HT were found to form local network aggregates characterized by the mass fractal dimension of ca. 2.5. Upon prolonged aging at room temperature, the originally viscous liquid solution transformed into a gel, in which a rodlike entity with the cross-sectional radius of gyration of 7.31 nm was disclosed. Real-space observation of the morphology of the film cast from the gel revealed the presence of long nanowhiskers. The fact that the width and height of these whiskers closely agreed with those of the rodlike entity in the gel deduced from model fitting of the SAXS profile indicated that the nanowhiskers were present in the wet gel. Time-resolved SAXS experiment revealed that the nanowhisker formation was accompanied by the crystallization of P3HT. The ultimate crystallinity attained in the nanowhiskers was only 32%, and the limited crystallizability was attributed to the network aggregate structure formed by P3HT prior to the gelation. The integrity of the nanowhiskers was largely maintained by the crystallinity of P3HT, as the dissipation of the nanowhisker morphology upon heating was found to occur concurrently with the melting of P3HT crystallites that led to homogenization of the solution.

Introduction

Poly(3-alkylthiophene)s (P3AT) are among the most widely used conjugated polymers for applications as the active materials in polymer solar cells and thin film transistors.^{1,2} In the solid state, P3ATs with high regioregularity are crystalline with the melting points tailored by the alkyl chain length.^{3,4} Crystallinity along with well-controlled crystal orientation is desirable for obtaining high charge mobility in the active layer composing of P3ATs.^{5,6} Poly(3-hexylthiophene) (P3HT) is one of the mostly studied members of P3AT with the crystal structure characterized by the monoclinic unit cell with space group *P2₁/c*.⁷ Within the crystal, the thiophene backbone and hexyl side chains of P3HT stack alternately along *a*-axis and the $\pi-\pi$ stacking of the thiophene rings is along *b*-axis. The nominal melting point of P3HT crystallite was typically above 200 °C.⁸

The fabrication of optoelectronic devices using conjugated polymers involves a solution processing, where the polymers are dissolved in a common organic solvent followed by film-casting (e.g., spin-casting) to form the active layer. It has been reported that the films of P3HT exhibited nanowhisker or nanowire morphology when they were cast directly from the solution with a poor solvent⁹ or subjected to a post-treatment by solvent vapor.¹⁰ The whiskers were usually long plate in shape, with micrometers in length, tens of nanometers in width, and only several nanometers in thickness.^{9–12} Further studies have revealed the crystalline nature and chain packing within the

nanowhiskers, where the crystalline P3HT backbones were found to lie normal to the whisker length.¹¹ Therefore, the nanowhisker formation is closely associated with the crystallization of P3HT,^{10–13} that is, the crystallization is driven by a liquid–solid phase separation in the solution with sufficiently poor solvent quality or by the enhancement of chain mobility due to penetration of solvent vapor into the films with disorganized morphology. In the former case, the crystalline whiskers generated in the solution may be transferred to the film upon rapid solvent removal. The photovoltaic devices with P3HT nanowhisker morphology was found to exhibit much higher power conversion efficiency than those with disorganized morphologies.^{9,14} Consequently, identifying the condition for generating P3HT nanowhiskers is also of practical importance for solar cell application of the material.

The present work focuses on the formation and thermally induced disruption of the nanowhiskers in P3HT/xylene gel studied *in situ* by small-angle X-ray scattering (SAXS). Like other conjugated polymer systems, the solutions of P3HT with the solvents of moderate or poor quality can undergo gelation when the polymer concentration is sufficiently high (e.g., in the semidilute regime).^{13,15–18} Xylene is a relatively poor solvent for P3HT in view of the larger difference in their solubility parameters (cf. $\delta_{\text{xylene}} = 17.95 \text{ J}^{0.5}/\text{cm}^{1.5}$; $\delta_{\text{P3HT}} = 19.27 \text{ J}^{0.5}/\text{cm}^{1.5}$)¹⁹ comparing with that of other common organic solvents (e.g., $\delta_{\text{chloroform}} = 18.96 \text{ J}^{0.5}/\text{cm}^{1.5}$; $\delta_{\text{dichlorobenzene}} = 19.58 \text{ J}^{0.5}/\text{cm}^{1.5}$). The study of Malik et al.¹³ provided the first insight into the gelation mechanism of P3HT/xylene solution. Crystalline fibrils constituting a network structure were observed from the TEM and SEM

*To whom correspondence should be addressed. E-mail: hlchen@che.nthu.edu.tw (H.-L.C.); kelvenc@mail.ksu.edu.tw (J.-H.C.).

micrographs of the dried gels; therefore, it was suggested that the crystallites acted as the cross-linking junctions to yield the gel property. It was noted in the paper that this conclusion was made based on the assumption that the morphology in the wet gel was not perturbed upon drying for carrying out the *ex-situ* microscopy experiment.

To probe the structure of the wet gel *in situ*, here we undertake a SAXS study for the gel formed by prolonged room-temperature aging of a semidilute P3HT/xylene solution originally prepared at elevated temperature. It will be shown that the gelation results in a strong enhancement of SAXS intensity and the change of scattering profile indicates a transformation of the structure from network aggregates formed by P3HT rodlike segments to long semicrystalline nanowhiskers that may form macroscopic network to yield the gel property. The time-resolved and temperature-dependent SAXS experiments demonstrate the close connection between the nanowhisker formation/disruption and crystallization/melting of P3HT in the solution.

Experimental Section

P3HT used here was synthesized by the Grignard metathesis according to the procedure reported in the literature.^{20,21} The polymer synthesized had a high regioregularity (> 95%), and its number-average molecular weight and polydispersity index were 17 600 g/mol and 1.24, respectively. The 1.6 wt % solution of P3HT and xylene was prepared by stirring their mixtures at ca. 70 °C for 12 h, where macroscopically homogeneous solutions were observed by naked eyes. The gel was then obtained by aging the solution at ca. 25 °C for a sufficiently long time (> 48 h).

The SAXS experiments were performed at the Endstation BL23A1 of the National Synchrotron Radiation Research Center (NSRRC), Taiwan, or using an in-house Bruker Nanostar SAXS instrument.^{22,23} For the synchrotron SAXS experiment, the energy of X-ray source and sample-to-detector distance were 14 keV and 2259 mm, respectively. The scattering signals were collected by MarCCD detector of 512 × 512 pixel resolution. For the in-house experiment, the wavelength of X-ray source and sample-to-detector distance were 0.154 nm (Cu k_{α}) and 65 cm (for the low- q configuration) or 23 cm (for the high- q configuration), respectively. The scattering intensity profile was output as the plot of the scattering intensity (I) vs the scattering vector, $q = (4\pi/\lambda) \sin(\theta/2)$ (θ = scattering angle), after corrections for solvent background, sample transmission, empty cell transmission, empty cell scattering, and the detector sensitivity.

The real-space morphologies of the thin films cast from the freshly prepared P3HT/xylene solution and the gel were observed using a Park System XE-70 scanning probe microscopy operated under noncontact mode. The thin films were prepared by spin-casting on wafer substrate with the spin rate of 800 rpm for 20 s followed by 3000 rpm for another 20 s.

The UV-vis absorption spectra of P3HT/xylene solution and gel were measured using a Hitachi U-3010 spectrophotometer. The samples were sandwiched between two microscope cover glasses to obtain the solution or gel layers of about 100 μm in thickness. The reported absorbances of the samples have been corrected for the solvent background. The photoluminescence (PL) spectra were recorded by using a Perkin-Elmer LS55 spectrophotometer. The samples were placed in sealed glass tubes with the thickness of 1 cm for the measurements. The excitation wavelength was 320 nm.

The endothermic event associated with the melting of P3HT crystallites was recorded by a TA Instruments 2000 differential scanning calorimeter. The gel samples were equilibrated at -5 °C and then heated to 110 at 10 °C/min for recording the melting endotherm.

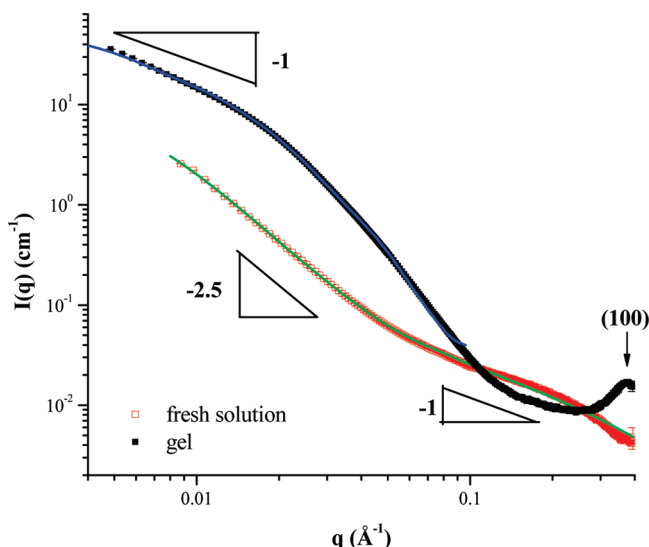


Figure 1. SAXS profiles of freshly prepared 1.6 wt % P3HT/xylene solution and the gel obtained by aging the solution at room temperature for 48 h. The solid curves represent the fits by the model of fractal structure factor coupled with cylinder form factor (for the fresh solution) and form factor of cylinder with elliptic cross section (for the gel).

Results and Discussion

Figure 1 shows the room-temperature SAXS profiles in a double-logarithmic plot of the freshly prepared P3HT/xylene solution and the gel. The scattering intensity of the fresh solution displays the power-law dependence of $q^{-2.47}$ in the low- q region ($q < 0.05 \text{ \AA}^{-1}$) followed by a q^{-1} dependence at higher q ($0.05 \text{ \AA}^{-1} < q < 0.2 \text{ \AA}^{-1}$) and finally a steeper intensity drop at $q > 0.2 \text{ \AA}^{-1}$. The observed scattering pattern closely resembles that of poly(2,3-diphenyl-5-hexyl-1,4-phenylenevinylene)/chloroform solution,²⁴ in which the conjugated polymer chains associated with form local network aggregates (of μm in size), and the subchains between the physical junctions in the aggregates were essentially rodlike. In this case, the power-law dependence in the low- q region reflects the mass fractal dimension of the aggregates while the rodlike segments constituting the aggregates give rise to q^{-1} dependence for the high- q intensity. Therefore, a model based on the coupling of fractal structure factor and cylinder form factor^{25,26} was adopted to fit the scattering profile of the fresh solution. The scattering intensity in this model is expressed by the following equation

$$I(q) = n\Delta\rho^2 S(q)P_{\text{cyl}}(q) \quad (1)$$

where n and $\Delta\rho$ is number density and scattering length density contrast of the cylinder, respectively. $S(q)$ is the structure factor given by²⁵

$$S(q) = 1 + \frac{D \exp[\Gamma(D-1) \sin(D-1) \tan^{-1}(q\xi)]}{(qR_e)^D [1+(q\xi)^{-2}]^{(D-1)/2}} \quad (2)$$

where D is the fractal dimension, ξ is the correlation length that can be used as a measure for the size of the fractal network aggregate, and R_e is the effective radius of the building block. ξ and R_e may be considered as the maximum and the minimum length scale, respectively, between which the fractal object exhibits the feature of self-similarity. That is, between these two characteristic length scales the scattering intensity of the fractal object shows the power-law dependence of $I(q) \sim q^{-D}$. $P_{\text{cyl}}(q)$ is the form factor of randomly oriented cylinders (with the radius

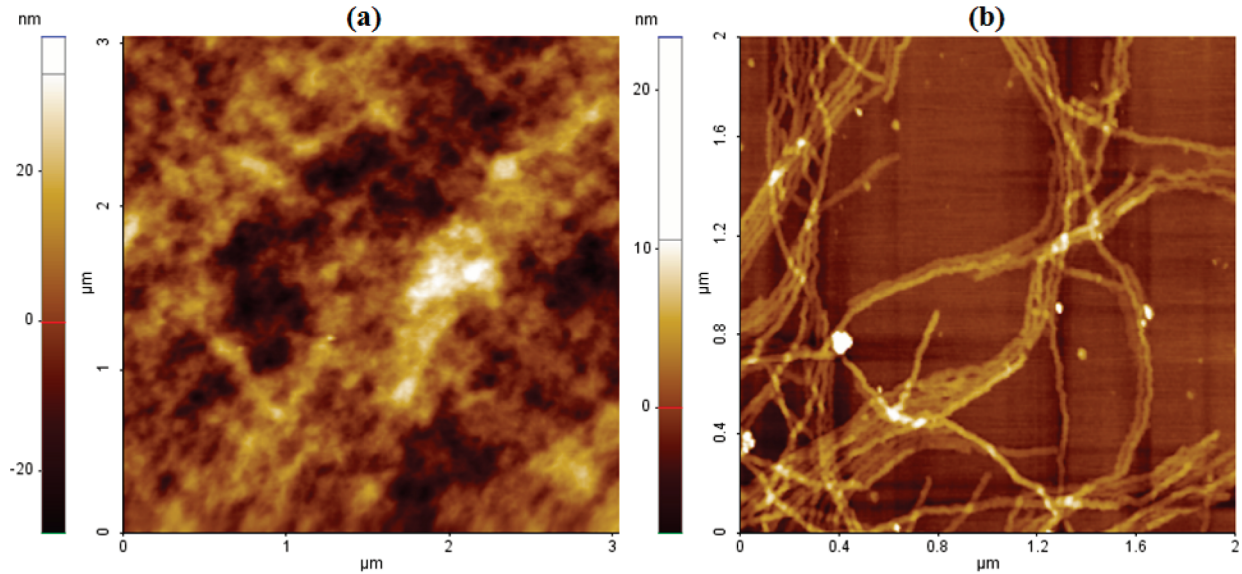


Figure 2. AFM topographic images of the film spin-cast from (a) 1.6 wt % fresh solution and (b) gel.

and length of R and L , respectively) given by²⁶

$$P_{\text{cyl}}(q) = V^2 \int_0^{\pi/2} \left(\frac{\sin\left(\frac{qL}{2}\cos\varphi\right)}{\frac{qL}{2}\cos\varphi} \right)^2 \left(\frac{2J_1(qR\sin\varphi)}{qR\sin\varphi} \right)^2 \sin\varphi \, d\varphi \quad (3)$$

The fitted result is displayed by the solid curve superposing on the corresponding experimental data in Figure 1. The fractal dimension of the aggregates, the average length of the rodlike segments between the physical junctions, and the radius of the segments obtained from the fit are 2.47 , 13.1 ± 0.12 nm, and 0.47 ± 0.03 nm, respectively. The segmental radius is in the typical range of that found for hairy-rod conjugated polymers such as poly(9,9-diethylfluorene) (PF8; $R = 0.33$ nm)²⁷ and poly(2-methoxy-5-(2'-ethylhexyloxy)-1,4-phenylenevinylene) (MEH-PPV; $R = 0.46$ nm).²⁸

The gel is found to exhibit significantly higher scattering intensity than the fresh solution. Here the intensity approaches q^{-1} dependence in the low- q region ($q < 0.02 \text{ \AA}^{-1}$), and a steep drop is observed at higher q . The scattering pattern signifies the presence of a rodlike entity with large cross section in the gel, where the steep intensity drop at $q > 0.02 \text{ \AA}^{-1}$ is due to the scattering contribution from the rod cross section. The rods are also very long such that the Guinier region containing the information on the average radius of gyration is not accessible under the q -range of the SAXS configuration. In the tail region of the SAXS profile, a peak corresponding to the (100) diffraction of P3HT crystallite is discernible,²⁹ implying the presence of crystallinity in the rods. The degree of crystallinity (normalized by the weight fraction of P3HT) calculated from the enthalpy of melting (using 99 J/g as the enthalpy of melting of 100% crystalline P3HT)¹³ measured using the gel sample is ca. 32%. The reliability of the measured crystallinity is confirmed by the close agreement to the crystallinity (ca. 34%) of the dried sample prepared by rapid drying of the original wet gel in a vacuum oven at 30 °C.

On basis of the previous studies showing that P3HT could form nanowhiskers with long plate geometry in solution with poor solvent,^{9,12,13} we attribute the rod entity probed by SAXS to the nanowhiskers developed in the gel. This is supported by the

real-space observation of the morphology of the thin film cast from the gel by AFM. For this experiment, the thin film was prepared by spin-casting because the very rapid solvent evaporation may allow the characteristic structure of the polymer in the gel to be effectively arrested. Figure 2 presents the topographic images of P3HT films on wafer cast from the freshly prepared solution and gel. The image of the film cast from fresh solution shows the typical aggregates of P3HT with mean-square roughness of 9.43 nm without obvious higher-order self-assembled structure (Figure 2a). By contrast, nanowhiskers are clearly observed for the film cast from the gel (Figure 2b). The average height and width of the individual whiskers measured from the topographic image are 5.0 and 24 nm, respectively. The observed height is similar to the previously reported value,^{9–11} but the width is significantly smaller. It can be seen in Figure 2b that the nanowhiskers appear to pack laterally to form bundles. A bundling of the whiskers may hence take place at a certain stage of solvent removal, driven by the excluded volume interaction between rod objects that leads to formation of a nematic phase. When the interfaces between two nanowhiskers are sufficiently close, the amorphous regions near the interfaces of them may merge to weld the whiskers. (It is more difficult for the crystalline regions to coalesce together due to the requirement of orientation matching of crystal surface.) Consequently, the width of the nanowhiskers eventually observed in the dry film becomes larger than that of the individual ones formed in the wet solution or gel.

It is noted that nanowhisker morphology is found to spread over nearly the entire area of the film from the gel, while the morphological feature found in the film cast from fresh solution is not clearly identified. Moreover, the degree of crystallinity of the dried gel determined from the enthalpy of melting is almost identical to that found for the wet gel. This means that most P3HT chains in the gel self-assemble to form nanowhiskers. Because the overall crystallinity is only 32%, the nanowhiskers should be semicrystalline containing both crystalline and amorphous regions.

Considering the plate shape of the nanowhiskers, the observed SAXS profile of the gel was fitted by the form factor of cylinder with elliptic cross section,³⁰ which serves as an approximation model for the system. The form factor function is given by³⁰

$$P(q) = V^2 \int_0^1 \psi_{\text{cc}}(q, a\sqrt{1-x^2}) \Lambda^2(qHx/2) \, dx \quad (4)$$

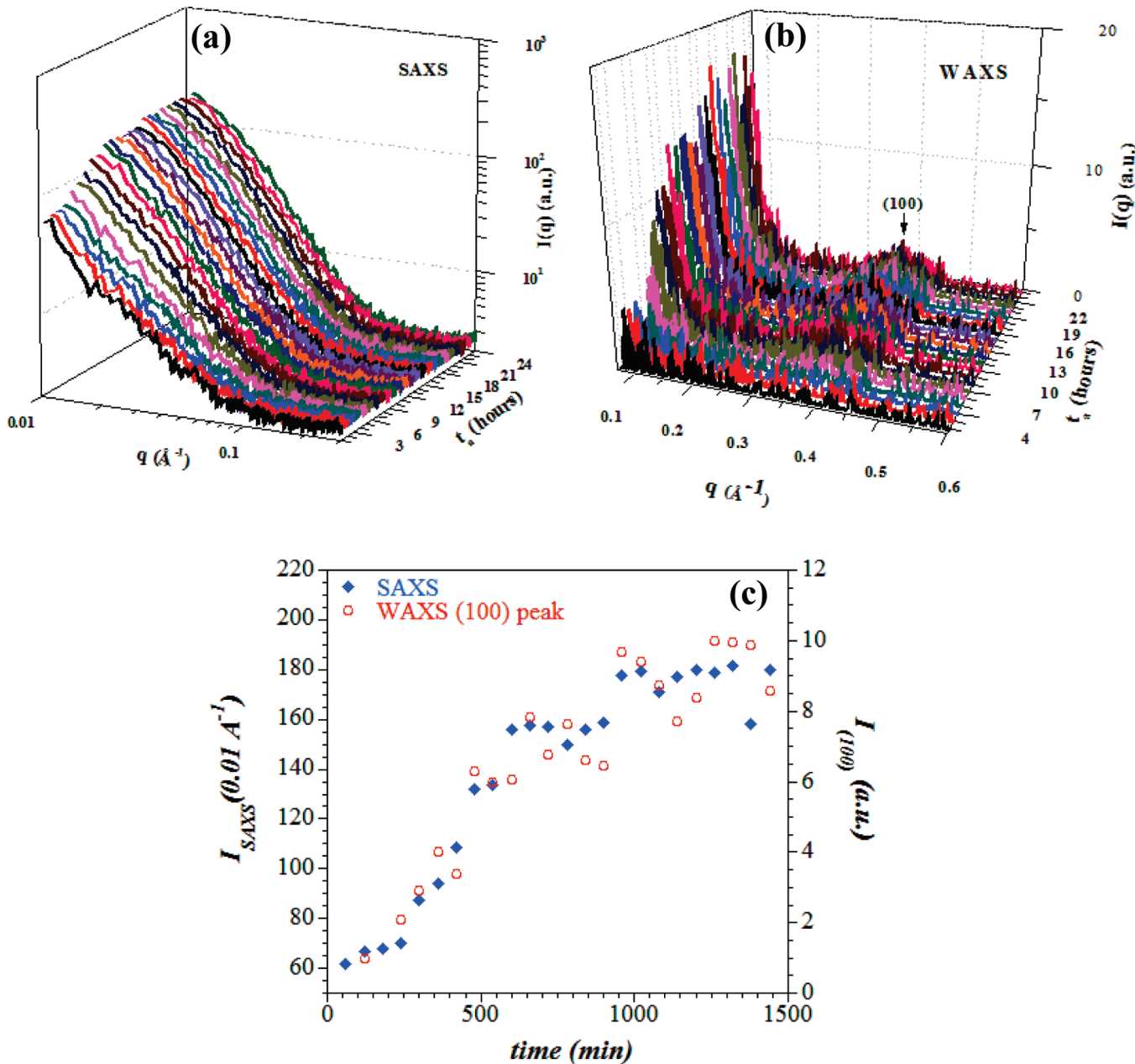


Figure 3. Time-resolved (a) SAXS and (b) WAXS profiles for monitoring the developments of nanowhiskers and crystallinity of P3HT, respectively, during the room-temperature aging of 1.6 wt % P3HT/xylene solution. (c) shows the concurrent growths of the SAXS intensity at 0.01\AA^{-1} and the (100) peak in the WAXS profile.

where

$$\psi_{\text{ec}}(q, a) = \frac{1}{\pi} \int_0^\pi \Lambda^2 \left(qa \sqrt{\frac{1+v^2}{2} + \frac{1-v^2}{2} \cos(y)} \right) dy \quad (5)$$

$$\Lambda(t) = J_1(t)/t \quad (6)$$

where H is the length of the cylinder, a is the minor radius of the elliptic cross section, and v is ellipticity defined as the ratio of the major radius to minor radius. The fitted result is displayed by the solid curve superposing on the experimental data in Figure 1. It can be seen that the model adopted provides a satisfactory fit to the data. The fitting yields the values of the minor and major radius of the elliptic cross section as 3.6 ± 0.002 and 12.1 ± 0.006 nm, respectively. Consequently, the width, height, and the

cross-sectional radius of gyration (R_c) of the nanowhiskers is 24.2, 7.2, and 7.31 nm, respectively. The smaller height measured by the *ex-situ* AFM comparing to that obtained from *in-situ* SAXS is attributed to the collapse of the nanowhiskers in the height direction upon solvent evaporation.

Time-resolved SAXS and wide-angle X-ray scattering (WAXS) experiments were carried out during the room-temperature aging of P3HT/xylene solution to monitor the structural development during gelation. As the aging progresses, the SAXS intensity in the low- q region is seen to grow concomitantly with the (100) crystalline peak in the WAXS profile (Figure 3), signaling that the nanowhisker formation is accompanied by crystallization. In contrast to the previous study showing that the P3HT nanowhiskers formed in dilute solution were highly crystalline,¹² the crystallinity of the whiskers in the present gel is quite low. We attribute the limited crystallizability to the precursory structure formed by P3HT in the solution prior to the

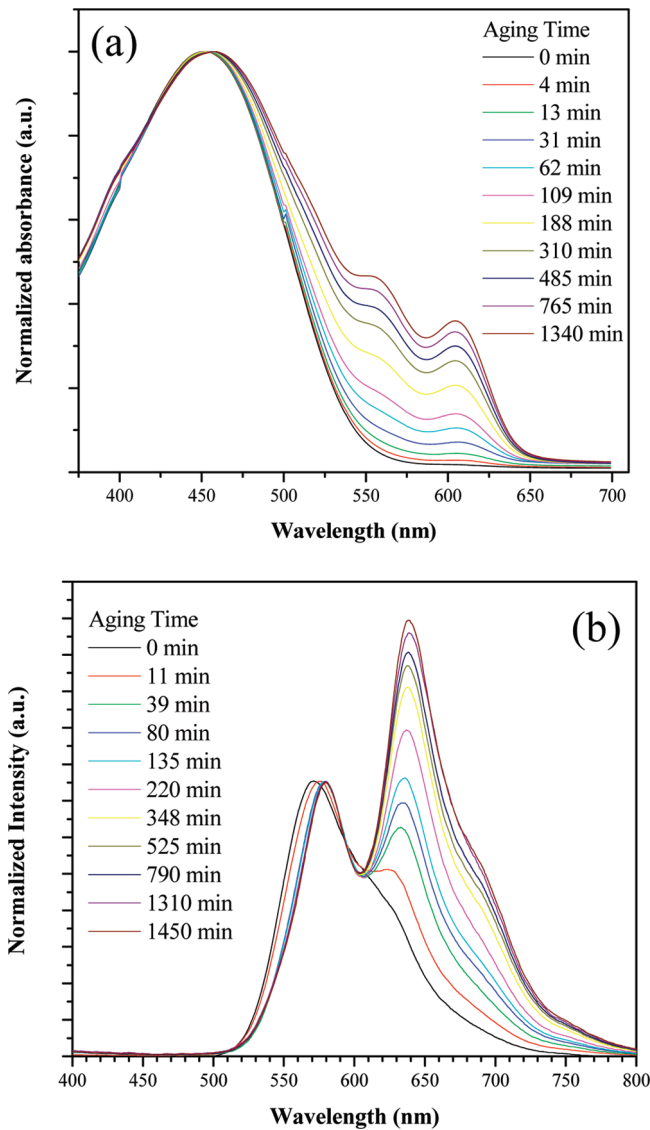


Figure 4. Time-dependent (a) UV-vis and (b) PL spectra of 1.6 wt % P3HT/xylene solution during aging at room temperature.

aging. The SAXS profile in Figure 1 shows that P3HT chains form network aggregates in the solution. The crystallization of P3HT within these aggregates can proceed more rapidly than the case where the chains are uniformly dispersed in the solution since the local polymer concentration is significantly higher than the overall concentration (i.e., 1.6 wt %). However, the entanglement and $\pi-\pi^*$ association may pin the P3HT chains together and hence hinder the registry and organization of a fraction of chains into the crystallites. As a consequence, the crystallinity attained is low.

Figure 4a displays the change of UV-vis absorption spectrum during the aging process. The spectrum of the fresh solution (aging time = 0 min) shows a peak at 453 nm associated with the $\pi-\pi^*$ transition of the dissolved chains in the solution.^{13,31} As the aging progresses, two additional peaks at 610 and 562 nm gradually develop, which can be assigned to 0–0 transition and a vibronic sideband,³¹ respectively, associated with P3HT in the ordered state.^{13,31} This vibronic coupling in the ordered state of P3HT is due to the interchain interaction involved in aggregation, gelation, and crystallization.³¹ The change of PL spectrum during aging is shown in Figure 4b. It can be seen that the crystallization during aging induces the development of two additional emission peaks at 640 and 700 nm. The formation of red-shifted emission

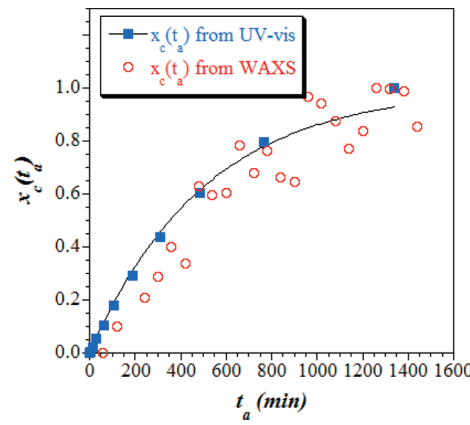


Figure 5. Development of relative crystallinity in 1.6 wt % P3HT/xylene solution during aging at room temperature. The crystallinities were calculated from the absorbance of the UV-vis peak at 610 nm and the integrated intensity of (100) diffraction peak in WAXS profile. The solid curve represents the fit of the data from UV-vis spectra by the exponential function, $x_c(t_a) = 1 - \exp(-kt_a)$.

peaks in PL spectrum is a well-known consequence of the improved electron delocalization in the solid state or good intermolecular ordering in semicrystalline conjugated polymers.^{32–34}

We assume that the absorbance of the UV-vis peak at 610 nm is directly proportional to the crystallinity of P3HT formed during aging; the relative crystallinity at a given aging time t_a can then be calculated by

$$x_c(t) = \frac{A_{610\text{nm}}(t_a) - A_{610\text{nm}}(0)}{A_{610\text{nm}}(\infty) - A_{610\text{nm}}(0)} \quad (7)$$

The relative crystallinity thus calculated is plotted against the aging time (t_a) in Figure 5 along with that determined from the intensity of (100) peak in WAXS profile. In contrast to the conventional sigmoidal curve found for polymer crystallization, the crystallinity development of P3HT during aging is found to closely follow the simple exponential function, $x_c(t_a) = 1 - \exp(-kt_a)$, as demonstrated by the fitting (the solid curve) of the experimental data by this equation. This exponential function indeed corresponds to the Avrami equation with the characteristic exponent n of 1.^{35,36} In the case of instantaneous nucleation, the close proximity of n to the value of 1.0 signals a one-dimensional fiberlike growth of the crystallites and is consistent with the formation of nanowhisker morphology.

Macroscopically, P3HT/xylene gel is found to turn into viscous solution upon heating to ca. 50 °C. The structural change associated with such a heating process is also investigated by SAXS here. Figure 6a presents the temperature-dependent SAXS profiles collected *in situ* by heating the gel. It can be seen that the SAXS intensity in the low- q region (e.g., at 0.01 Å⁻¹) decreases progressively with increasing temperature, and the intensity drops abruptly at ca. 50 °C (Figure 6c), signaling the disruption of the nanowhisker morphology upon heating. The reduction of SAXS intensity occurs almost concurrently with the decrease of the integrated intensity of (100) peak (Figure 6c) and is consistent with the crystallite melting curve probed by DSC (Figure 6b) and the diminishment of 640 and 700 nm peaks in the PL spectra. This means that the integrity of the nanowhiskers is largely maintained by the crystallinity of P3HT, such that the nanowhisker morphology is disrupted upon heating to the crystal melting point. Within the semicrystalline nanowhisker the crystallites may act as the physical cross-links which restrict the degree of swelling of the amorphous chains and hence retain the integrity of the nanowhisker. When the crystallites melt, more solvent molecules are allowed to penetrate into the whisker to dissolve the amorphous

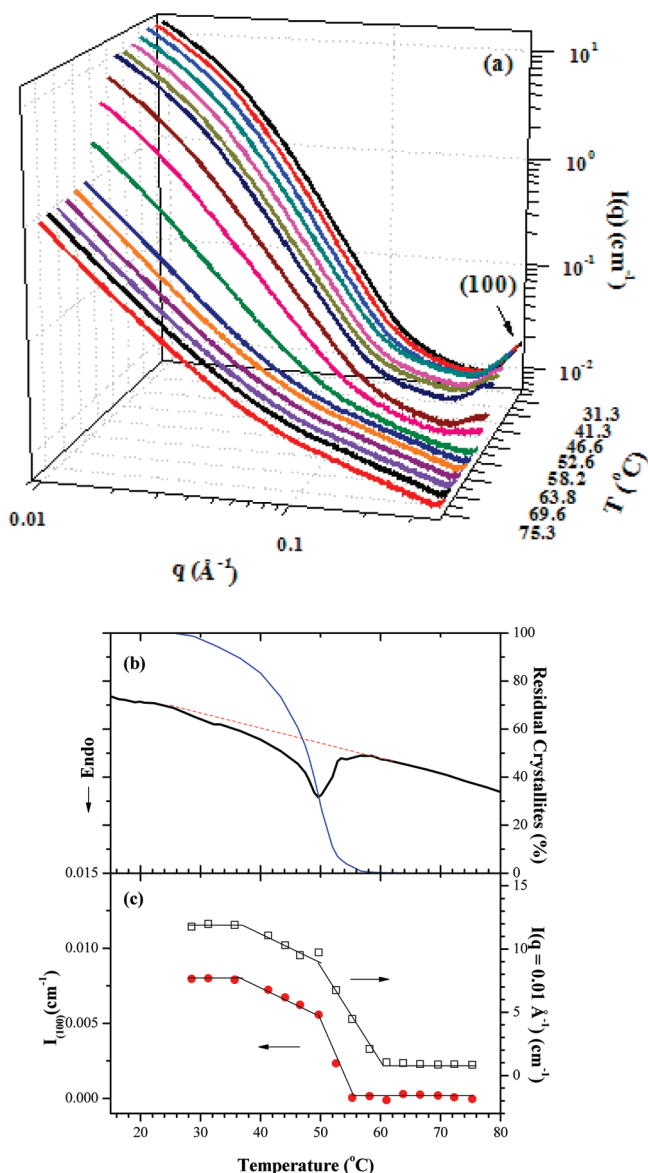


Figure 6. (a) Temperature-dependent SAXS profiles of P3HT/xylene gel collected in a heating cycle, (b) the melting curve of the gel recorded by DSC (heating rate = 10 °C/min), and (c) the dependences of the SAXS intensity at $q = 0.01\text{ \AA}^{-1}$ and the integrated intensity of (100) peak. The reduction of SAXS intensity occurs almost concurrently with the decrease of the integrated intensity of (100) peak and is consistent with the crystallite melting curve probed by DSC.

P3HT chains into the bulk solution; as a result, the nanowhisker is disintegrated.

Conclusion

We have demonstrated that SAXS can be used to identify the formation of nanowhiskers in the gel composing of P3HT. Because of the convenience of conducting time-resolved and *in-situ* experiments, this tool should be useful for probing the formation mechanism of this unique morphology of P3ATs. Here we have shown that the P3HT chains originally forming network aggregates in xylene solution underwent crystallization to yield the nanowhiskers. The networking of the nanowhiskers may lead to gelation of the solution. In contrast to the highly crystalline nanowhiskers formed in dilute P3HT solutions, the whiskers in the gel showed relatively low crystallinity due to the strong interchain interaction of P3HT in the network aggregates that restricted the registry and organiza-

tion of a fraction of chains into the crystallites. The integrity of the nanowhiskers was largely maintained by the crystallinity of P3HT; therefore, the nanowhisker morphology was disrupted upon heating to the melting point of P3HT crystallites.

Acknowledgment. We acknowledge the financial support of the National Science Council of the Republic of China under Grants NSC 97-2752-E-002-PAE and NSC 98-2221-E-168-002.

References and Notes

- Thompson, B. C.; Fréchet, J. M. J. *Angew. Chem., Int. Ed.* **2008**, *47*, 58–77.
- Sirringhaus, H.; Brown, P. J.; Friend, R. H.; Nielsen, M. M.; Bechgaard, K.; Langeveld-Voss, B. M. W.; Spiering, A. J. H.; Janssen, R. A. J.; Meijer, E. W.; Herwig, P.; de Leeuw, D. M. *Nature* **1999**, *401*, 685–688.
- Joshi, S.; Grigorian, S.; Pietsch, U. *Phys. Status Solidi A* **2008**, *205*, 488–496.
- Brinkmann, M.; Rannou, P. *Macromolecules* **2009**, *42*, 1125–1130.
- Jimison, L. H.; Toney, M. F.; McCulloch, I.; Heeney, M.; Salleo, A. *Adv. Mater.* **2009**, *21*, 1568–1572.
- Zhang, R.; Li, B.; Lovu, M. C.; Jeffries-EL, M.; Sauvé, G.; Cooper, J.; Jia, S.; Tristram-Nagle, S.; Smilgies, D. M.; Lambeth, D. N.; McCullough, R. D.; Kowalewski, T. *J. Am. Chem. Soc.* **2006**, *128*, 3480–3481.
- Kayunkid, N.; Uttiya, S.; Brinkmann, M. *Macromolecules* **2010**, *43*, 4961–4967.
- Malik, S.; Nandi, A. K. *J. Polym Sci. Part B: Polym. Phys.* **2002**, *40*, 2073–2085.
- Berson, S.; De Bettignies, R.; Bailly, S.; Guillerez, S. *Adv. Funct. Mater.* **2007**, *17*, 1377–1384.
- Kim, D. H.; Park, Y. D.; Jang, Y.; Kim, S.; Cho, K. *Macromol. Rapid Commun.* **2005**, *26*, 834–839.
- Ihn, K. J.; Moulton, J.; Smith, P. *J. Polym. Sci., Part B: Polym. Phys.* **1993**, *31*, 735–742.
- Liu, J. H.; Arif, M.; Zou, J. H.; Khondaker, S. I.; Zhai, L. *Macromolecules* **2009**, *42*, 9390–9393.
- Malik, S.; Jana, T.; Nandi, A. K. *Macromolecules* **2001**, *34*, 275–282.
- Xin, H.; Kim, F. S.; Jenekhe, S. A. *J. Am. Chem. Soc.* **2008**, *130*, 5424–5425.
- Chen, J. H.; Chang, C. S.; Chang, Y. X.; Chen, C. Y.; Chen, H. L.; Chen, S. A. *Macromolecules* **2009**, *42*, 1306–1314.
- Huang, W. Y.; Huang, P. T.; Han, Y. K.; Lee, C. C.; Hsieh, T. L.; Chang, M. Y. *Macromolecules* **2008**, *41*, 7485–7489.
- Kitts, C. C.; Vanden Bout, D. A. *Polymer* **2007**, *48*, 2322–2330.
- Wang, P. S.; Lu, H. H.; Liu, C. Y.; Chen, S. A. *Macromolecules* **2008**, *41*, 6500–6504.
- Van Krevelen, D. W. *Properties of Polymers*; Elsevier Science Publishers: Amsterdam, 1972.
- Loewe, R. S.; Khersonsky, S. M.; McCullough, R. D. *Adv. Mater.* **1999**, *11*, 250–253.
- Loewe, R. S.; Ewbank, P. C.; Liu, J. S.; Zhai, L.; McCullough, R. D. *Macromolecules* **2001**, *34*, 4324–4333.
- Jeng, U. S.; Su, C. H.; Su, C. J.; Liao, K. F.; Chuang, W. T.; Lai, Y. H.; Chang, J. W.; Chen, Y. J.; Huang, Y. S.; Lee, M. T.; Yu, K. L.; Lin, J. M.; Liu, D. G.; Chang, C. F.; Liu, C. Y.; Chang, C. H.; Liang, K. S. *J. Appl. Crystallogr.* **2010**, *43*, 110–121.
- Nandan, B.; Lee, C. H.; Chen, H. L.; Chen, W. C. *Macromolecules* **2005**, *38*, 10117–10126.
- Li, Y. C.; Chen, K. B.; Chen, H. L.; Hsu, C. S.; Tsao, C. S.; Chen, J. H.; Chen, S. A. *Langmuir* **2006**, *22*, 11009–11015.
- Chen, S. H.; Teixeira, J. *Phys. Rev. Lett.* **1986**, *57*, 2583–2586.
- Glatter, O.; Kratky, O. *Small Angle X-ray Scattering*; Academic Press: London, 1982.
- Rahman, M. H.; Chen, C. Y.; Liao, S. C.; Chen, H. L.; Tsao, C. S.; Chen, J. H.; Liao, J. L.; Ivanov, V. A.; Chen, S. A. *Macromolecules* **2007**, *40*, 6572–6578.
- Ou-Yang, W. C.; Chang, C. S.; Chen, H. L.; Tsao, C. S.; Peng, K. Y.; Chen, S. A.; Han, C. C. *Phys. Rev. E* **2005**, *72*, 031802.

- (29) Tashiro, K.; Ono, K.; Minagawa, Y.; Kobayashi, M.; Kawai, T.; Yoshino, K. *J. Polym Sci., Part B: Polym. Phys.* **1991**, *29*, 1223–1233.
- (30) Guinier, A.; Fournet, G. *Small-Angle Scattering of X-Rays*; John Wiley: New York, 1955.
- (31) Rughooopath, S. D. D. V.; Hotta, S.; Heeger, A. J.; Wudl, F. *J. Polym. Sci., Part B: Polym. Phys.* **1987**, *25*, 1071–1078.
- (32) Österbacka, R.; An, C. P.; Jiang, X. M.; Vardeny, Z. V. *Science* **2000**, *287*, 839–842.
- (33) Brown, P. J.; Thomas, D. S.; Kohler, A.; Wilson, J. S.; Kim, J.-S.; Ramsdale, C. M.; Sirringhaus, H.; Friend, R. H. *Phys. Rev. B* **2003**, *67*, 064203.
- (34) Jiang, X. M.; Österbacka, R.; Korovyanko, O.; An, C. P.; Horovitz, B.; Janssen, R. A. J.; Vardeny, Z. V. *Adv. Funct. Mater.* **2002**, *12*, 587–597.
- (35) Avrami, M. *J. Chem. Phys.* **1939**, *7*, 1103–1112.
- (36) Avrami, M. *J. Chem. Phys.* **1941**, *9*, 177–184.